46th AIAA Aerospace Sciences Meeting and Exhibit
7 - 10 January 2008, Reno, Nevada

AIAA 2008-114

Analysis of an Ejector-Augmented Pulse Detonation Rocket

Donald R. Wilson,[1] Frank K. Lu,[2] JunHyun Kim[3] and Haider Hekiri[4]
University of Texas at Arlington, Arlington, Texas, 76019

A spreadsheet method for rapid estimation of the performance of ejector-augmented pulse detonation rocket (PDR) engines has been developed. The method integrates the Endo-Fujiwara analytic model of the PDR with a modified version of the ejector model developed by Heiser and Pratt. A quasi-steady ejector analysis is performed by solving the steady-state ejector equations at various time steps during the PDR cycle. Cycle-averaged performance is then obtained by averaging the performance parameters such as thrust augmentation ratio, specific thrust and specific impulse over the cycle. Applications of the spreadsheet model for design optimization of the integrated ejector-augmented PDR are presented to illustrate its design capabilities for specific flight conditions and for typical constant dynamic pressure trajectories.

I. Introduction

A NOVEL multi-mode propulsion system employing integration of several detonation-based combustion modes into a single flow path has been proposed for potential application to hypersonic cruise or single-stage-to-orbit (SSTO) vehicles. The multi-mode, pulse detonation propulsion system comprises of the following four modes of operation:

1. An ejector-augmented pulse detonation rocket (EJ/PDR) for take off to moderate supersonic Mach numbers,
2. A pulsed normal detonation wave engine (NDWE) mode for operation at flight Mach numbers from approximately 3 to 7, which corresponds to combustion chamber Mach numbers less than the Chapman–Jouguet (CJ) Mach number,
3. An oblique detonation wave engine (ODWE) mode of operation for flight Mach numbers that result in detonation chamber Mach numbers greater than the CJ Mach number, and
4. A pure PDR mode of operation at very high Mach numbers and altitudes.

The study presented in this paper involves Mode 1, the ejector-augmented pulse detonation rocket (EA/PDR). Several CFD simulations of the EA/PDR have been presented previously;[1-3] however, in this study, we develop an analysis model that can be implemented in an EXCEL spreadsheet to provide a preliminary design tool for investigating alternative design concepts and performing rapid performance estimates. The development of the model is described in detail, comparisons of results with experimental data and from CFD simulations are provided, several applications are presented to illustrate the design optimization capabilities of the code, and performance estimates for a typical constant dynamic pressure trajectory are given.

II. PDR Model

The cyclic operation of the basic PDR is depicted in Fig. 1. The cycle consists of several distinct events. Starting with the detonation chamber just after the combustion products of the previous cycle have been expelled (1), a valve is opened and the combustion chamber is filled with a fuel/oxidizer mixture (2). A valve seals the detonation chamber and the detonation initiator ignites the propellant mixture, causing a detonation to form at the closed end of the detonation tube (3). The detonation wave propagates through the chamber (4) and exits the combustion chamber, generating a series of rarefaction waves at the open end (5). The rarefaction waves travel from

[1] Professor and Chair, Mechanical and Aerospace Engineering Department, Box 19018. AIAA Associate Fellow.
[2] Professor and Director, Aerodynamics Research Center, Mechanical and Aerospace Engineering Department, Box 19018. AIAA Associate Fellow.
[3] Graduate Research Assistant, Mechanical and Aerospace Engineering Department, Box 19018.
[4] Graduate Research Assistant, Mechanical and Aerospace Engineering Department, Box 19018.

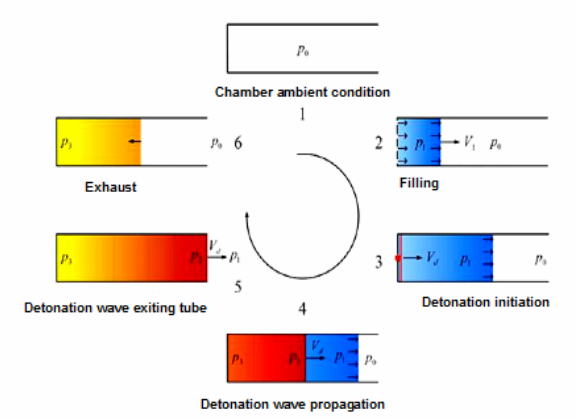

Figure 1. PDR cycle.

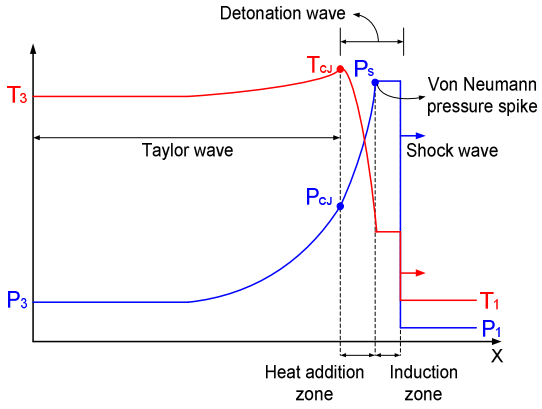

Figure 2. ZND model.

the open end to the closed end, causing the burned gas to exhaust (6). The pressure in the combustion chamber drops as the combustion products are expelled via a series of reflected expansion waves. Residual combustion products are purged from the chamber to prevent auto-ignition of the fresh fuel/oxidizer charge and the chamber is ready for the next fill cycle (6). For the following analysis, the cycle time is assumed to be the sum of four distinct processes: detonation, exhaust, purge, and refill.

A detonation chamber pressure and temperature profile based on the classical Zeldovich-von Neumann-Döring (ZND) model is shown schematically in Fig. 2 (adapted from Ref. 4). The shock front is moving from left to right into an unburned fuel-air mixture. The high pressure region of unburned gas behind the shock is known as the von Neumann spike. Following a short ignition delay, typically on the order of 1 μs, chemical reactions are initiated and the energy release causes a decrease in pressure and an increase in temperature to levels predicted from CJ theory. An unsteady expansion is generated at the closed end of the chamber to satisfy the zero velocity boundary condition which reduces the CJ pressure p_2 to the end-wall pressure p_3.

The von Neumann (VN) spike conditions are calculated by assuming a normal shock wave moves into the fuel-oxidizer mixture at a speed equal to the CJ velocity. Assuming a calorically perfect gas model, the VN spike conditions are given by the following equations

$$\frac{p_1}{p_o} = 1 + \frac{2\gamma_o}{\gamma_o + 1}\left(M_o^2 - 1\right) \tag{1}$$

$$\frac{\rho_1}{\rho_o} = \frac{\left(\gamma_o + 1\right)M_o^2}{2 + \left(\gamma_o - 1\right)M_o^2} \tag{2}$$

$$\frac{T_1}{T_o} = \frac{p_1}{p_o}\frac{\rho_o}{\rho_1} \tag{3}$$

where subscript o refers to the upstream unburnt state and subscript 1 refers to the VN state while M_o is the Mach number of the detonation wave referred to the upstream state. The CJ wave speed is calculated with the NASA Chemical Equilibrium Application (CEA) code.[5] Typical initial conditions are shown in Table 1, and the resulting VN and CJ conditions are given in Table 2.

The PDR analysis follows the model presented by Endo and Fujiwara.[6] In this model, the CJ detonation wave is assumed to be followed by a self-centered Taylor rarefaction wave whose front boundary coincides with the tail of the CJ wave. Therefore, the flow conditions at the front of the wave are the CJ conditions. The flow conditions inside the rarefaction wave are given by

$$p = \left(\frac{1}{\gamma_2} + \frac{\gamma_2 - 1}{\gamma_2} \frac{x}{x_2} \right)^{2\gamma_2/(\gamma_2 - 1)} p_2 \tag{4}$$

$$\rho = \left(\frac{1}{\gamma_2} + \frac{\gamma_2 - 1}{\gamma_2} \frac{x}{x_2} \right)^{2/(\gamma_2 - 1)} \rho_2 \tag{5}$$

$$u = u_2 - \left(\frac{2}{\gamma_2 + 1} \right) \left(\frac{x_2 - x}{t} \right) \tag{6}$$

$$a = a_2 - \left(\frac{\gamma_2 - 1}{\gamma_2 + 1} \right) \left(\frac{x_2 - x}{t} \right) \tag{7}$$

$$T = \frac{p}{\rho R_2} \tag{8}$$

Table 1. Typical initial conditions for detonation wave calculations.

Pressure p_o	Temperature T_o	Density ρ_o	Oxidizer	Fuel	Chemical equivalence ratio	Tube length L
1 atm	300 K	0.488 kg/m³	O_2	H_2	1	1 m

Table 2. Calculated VN and CJ conditions for entrance conditions listed in Table 1.

	Speed D_2, m/s	Pressure, atm	Temperature, K	Density, km/m^3	Mach No., M_{CJ}	γ	Gas constant, J/(kg.K)
VN	2835	32.06	1893	2.48	5.2562	1.4014	692.3
CJ	2835	18.06	3675	0.85	5.2562	1.1288	573.4

Pressure and temperature distributions within the tube at the time at which the detonation wave reaches the open end of the tube are shown in Fig. 3. Note that the temperature within the detonation chamber does not drop nearly as much as the pressure. At the rear of the rarefaction wave, the flow velocity $u_3 = 0$ in order to match the closed end-wall boundary condition. Thus the flow conditions at the trailing edge of the rarefaction wave are

$$x_3 = \frac{x_2}{2} \tag{9}$$

$$D_3 = a_3 = \frac{D_{CJ}}{2} \tag{10}$$

$$p_3 = \frac{\gamma_1}{2\gamma_2} \left(\frac{\gamma_2 + 1}{2\gamma_2} \right)^{(\gamma_2 + 1)/(\gamma_2 - 1)} M_{CJ}^2 p_o \tag{11}$$

$$\rho_3 = 2 \left(\frac{\gamma_2 + 1}{2\gamma_2} \right)^{(\gamma_2 + 1)/(\gamma_2 - 1)} \rho_o \tag{12}$$

$$T_3 = \frac{p_3}{\rho_3 R_3} \tag{13}$$

where $\gamma_1 = \gamma_o = 1.4014$, $\gamma_2 = 1.209$ and $R_3 = R_2 = 573.4$ J/(kg K).

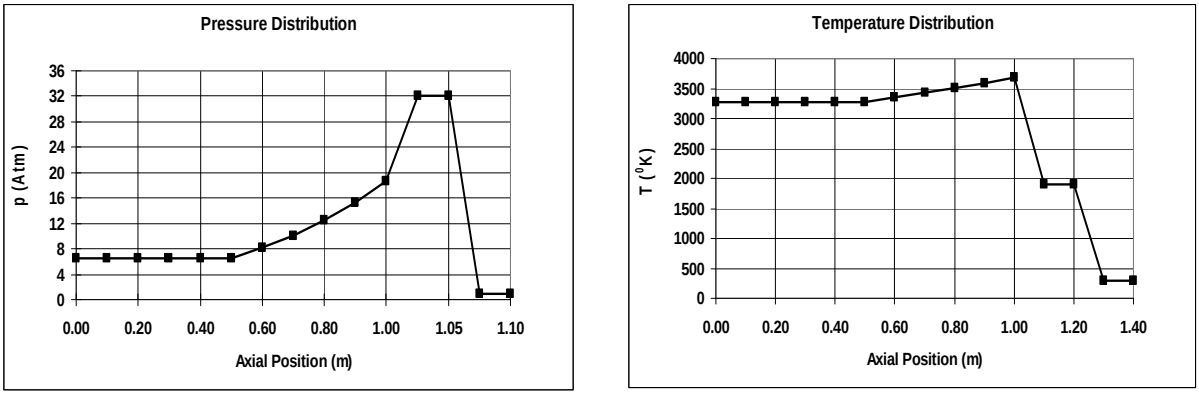

Figure 3. Pressure and temperature distribution at $t = t_1/2$.

Endo and Fujiwara assumed that the wave system exits the open end of the detonation tube at a time

$$t_1 = \frac{L}{D_3} = \frac{2L}{D_{CJ}} \tag{14}$$

which corresponds to a time of 0.71 ms for a 1 m tube length. At this time, the conditions within the detonation tube are characterized by a spatially uniform distribution of $u_3 = 0$, p_3, ρ_3 and T_3. During the combustion phase $(0 \le t \le t_1)$, the end-wall conditions are $p_{tp} = p_3$ and $T_{tp} = T_3$, which become the total pressure and total temperature conditions for the primary flow in the subsequent ejector analysis.

Following the departure of the trailing edge of the rarefaction wave from the open end of the tube, a reflected expansion wave travels from the open end to the closed end at a speed equal to the sonic speed a_3. Thus, the time required for the wave propagation from the open end to the closed end is given by

$$t_2 - t_1 = \frac{L}{D_3} = \frac{2L}{D_2} \tag{15}$$

yielding

$$t_2 = \frac{2L}{D_{CJ}} + t_1 = \frac{4L}{D_{CJ}} \tag{16}$$

noting that $D_2 = D_{CJ}$. For a tube of 1 m length, t_2 is 1.41 ms. The flow conditions inside the reflected rarefaction wave are given by

$$p = \left(1 + \frac{\gamma_2 - 1}{D_{CJ}} \frac{L - x}{t - t_1}\right)^{2\gamma_2/(\gamma_2 - 1)} p_{ex} \tag{17}$$

$$\rho = \left(1 + \frac{\gamma_2 - 1}{D_{CJ}} \frac{L - x}{t - t_1}\right)^{2/(\gamma_2 - 1)} \rho_{ex} \tag{18}$$

$$u = u_{ex} - \frac{2}{\gamma_2 + 1} \frac{L - x}{t - t_1} \tag{19}$$

$$a = a_{ex} + \frac{\gamma_2 - 1}{\gamma_2 + 1}\frac{L - x}{t - t_1} \tag{20}$$

where

$$p_{ex} = \frac{\gamma_1}{\gamma_2^{2\gamma_2/(\gamma_2-1)}(\gamma_2+1)} M_{CJ}^2 p_1 \tag{21}$$

$$\rho_{ex} = \left(\frac{\gamma_2 + 1}{\gamma_2^{(\gamma_2+1)/(\gamma_2-1)}}\right)\rho_1 \tag{22}$$

$$u_{ex} = a_{ex} = \frac{D_{CJ}}{\gamma_2 + 1} \tag{23}$$

The final phase of the blow down process is estimated by assuming a linear pressure decay

$$p_{tp} = (p_3 - p_o)\left(1 - \frac{t - t_2}{t_3 - t_2}\right) + p_o \tag{24}$$

where

$$t_3 = \frac{\rho_3 L}{\rho_{ex} u_{ex}} + t_1 \tag{25}$$

and

$$\rho_{ex} u_{ex} = \left(\frac{2}{\gamma_2 + 1}\right)^{(\gamma_2+1)/(\gamma_2-1)} \rho_3 a_3 \tag{26}$$

is the exhaust gas mass flow rate per unit area. Since the blow down occurs through multiple reflections of isentropic expansion waves, the temperature distribution during the blow down can be calculated from the isentropic relation

$$T_{tp} = T_3\left(\frac{p_{tp}}{p_3}\right)^{(\gamma_2-1)/\gamma_2} \tag{27}$$

The predicted end-wall pressure and temperature distributions are shown in Fig. 4. Note that p_{tp} and T_{tp} are equal to the constant p_3 and T_3 values during the time interval $0 \le t \le t_2$ and decay during the time interval $t_2 \le t \le t_3$. Also note that the temperature in the detonation chamber is still very high at the culmination of the blow down process, which agrees with previous CFD predictions and experimental observations, and illustrates the necessity for purging the residual combustion products prior to initiation of the next filling cycle. Otherwise, injection of a fresh fuel-oxidizer mixture into the detonation chamber will result in deflagration rather than detonation combustion,

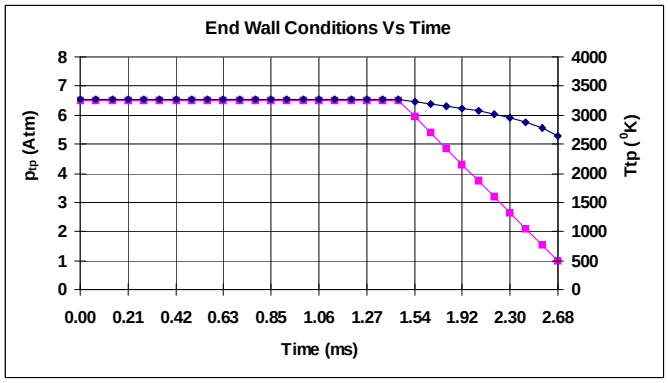

Figure 4. PDR end-wall conditions
(blue line – temperature, pink line – pressure).

since the temperature is greater than the auto-ignition temperature. The pressure and temperature distributions shown in Fig. 4 are used as the equivalent total pressure and temperature variations with time in the subsequent quasi-steady ejector analysis described in the next sectionThe total cycle time, excluding purge and refilling times, $t_{cycle} = t_1 + t_2 + t_3$, for the 1 m detonation tube length is 2.68 ms, which agrees to within 10 percent of the measured value from a recent test of in our 1 m detonation tube. Furthermore, the predicted end-wall pressure during the detonation phase of the cycle agrees with measured end-wall pressure distributions.

III. Ejector Model

The ejector model is based on an adaptation of the steady-state ejector model developed by Heiser and Pratt.7 The model is illustrated in Fig. 5, and is based on the following assumptions

1. The inlet primary flow will be supersonic
2. The inlet secondary flow will be subsonic
3. The ejector exit plane flow will be choked ($M_e = 1$)
4. The primary and secondary flows will be fully mixed at the inlet plane (Station *i*) with a uniform static pressure p_i
5. For supersonic flight, the inlet recovery will be estimated by using the Military Specification 5008B8

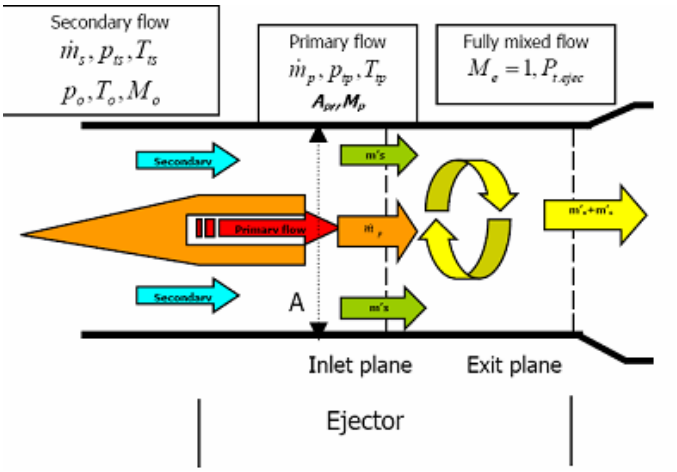

Figure 5. Ejector model.

$$\frac{p_{ts}}{p_{to}} = \pi_d = \pi_{d,max}\eta_r \tag{28}$$

where $p_{ts}/p_{to} = \pi_d = \pi_{d,max} =$ 0.96 and

$$\eta_r = 1 - 0.075(M_o - 1)^{1.35} \tag{29}$$

6. A perfect gas model is assumed, but the values for the gas constant and specific heat for the primary, secondary and mixed-flow streams are based on the appropriate temperature level and composition of the respective streams.

The primary stream input parameters are $p_{tp}/p_o = p_3/p_o$, $T_{tp}/T_o = T_3/T_o$, γ_p and R_p, whereas, for the secondary stream, the input parameters are $p_{ts}/p_o = \pi_D p_{to}/p_o$, $T_{tp}/T_o = T_{to}/T_o$, γ_s and R_s. The free stream pressure and temperature ratios are given by the isentropic relations

$$\frac{p_{ts}}{p_o} = \left(1 + \frac{\gamma_s - 1}{2} M_o^2\right)^{\gamma/(\gamma-1)} \tag{30}$$

$$\frac{T_{ts}}{T_o} = 1 + \frac{\gamma_s - 1}{2} M_o^2 \tag{31}$$

An iterative procedure is necessary to solve the resulting equations. Heiser and Pratt used the static pressure ratio p_i/p_o as the iteration variable. Assuming an isentropic expansion from the PDR total pressure p_{tp} to the static pressure p_i, the Mach number and area ratio for the primary flow are given by

$$M_{pi} = \left\{ \frac{2}{\gamma_p - 1} \left[\left(\frac{p_{tp}}{p_o} \frac{p_o}{p_i} \right)^{(\gamma_p - 1)/\gamma_p} - 1 \right] \right\}^{1/2} \tag{32}$$

$$\frac{A_{pi}}{A_p^*} = \frac{1}{M_{pi}}\left[\frac{2}{\gamma_p+1}\left(1+\frac{\gamma_p-1}{2}M_{pi}^2\right)^{(\gamma_p+1)/2[(\gamma_p-1)]}\right] \tag{33}$$

$$\frac{A_{pi}}{A} = \frac{A_{pi}}{A_p^*}\frac{A_p^*}{A} \tag{34}$$

Then assuming the secondary inlet flow also expands to the same static pressure ratio, p_i/p_o, the secondary stream Mach number at the inlet plane station is given by

$$M_{si} = \left\{\frac{2}{\gamma_s-1}\left[\left(\frac{p_{ts}}{p_o}\frac{p_o}{p_i}\right)^{(\gamma_s-1)/\gamma_s} - 1\right]\right\}^{1/2} \tag{35}$$

From the mass flow parameter,

$$\dot{m} = \rho A u = \frac{p}{RT}AM\sqrt{\gamma RT} = \frac{pAM\sqrt{\gamma/RT}}{\left(1+\frac{\gamma-1}{2}M^2\right)^{(\gamma+1)/[2(\gamma-1)]}} \tag{36}$$

the bypass ratio can be calculated as

$$\alpha = \frac{\dot{m}_s}{\dot{m}_p} = \frac{p_{ts}}{p_{tp}}\frac{A_{si}}{A_{pi}}\frac{M_{si}}{M_{pi}}\sqrt{\frac{T_{te}}{T_{ts}}\frac{\gamma_s}{\gamma_p}\frac{R_p}{R_s}}\frac{\left(1+\frac{\gamma_p-1}{2}M_{pi}^2\right)^{(\gamma_p+1)/[2(\gamma_p-1)]}}{\left(1+\frac{\gamma_s-1}{2}M_{si}^2\right)^{(\gamma_s+1)/[2(\gamma_s-1)]}} \tag{37}$$

Assuming complete mixing between the inlet plane and exit plane, conservation of energy yields the following relation for T_{te}/T_o

$$\frac{T_{te}}{T_o} = \frac{1}{1+\alpha}\frac{C_{pp}}{C_{pe}}\frac{T_{tp}}{T_o} + \frac{\alpha}{1+\alpha}\frac{C_{ps}}{C_{pe}}\frac{T_{ts}}{T_o} \tag{38}$$

where

$$C_{pe} = \frac{1}{1+\alpha}C_{pp} + \frac{\alpha}{1+\alpha}C_{ps} \tag{39}$$

$$C_{pp} = \frac{\gamma_p R_p}{\gamma_p - 1} \tag{40}$$

$$C_{ps} = \frac{\gamma_s R_s}{\gamma_s - 1} \tag{41}$$

Furthermore, since the flow is assumed to be choked at the exit plane ($M_e = 1$)

$$\frac{T_e}{T_{te}} = \left(1+\frac{\gamma_e-1}{2}M_e^2\right)^{-1} = \frac{2}{\gamma_e+1} \tag{42}$$

$$\frac{p_e}{p_{te}} = \left(1+\frac{\gamma_e-1}{2}M_e^2\right)^{-\gamma_e/(\gamma_e-1)} = \left(\frac{2}{\gamma_e+1}\right)^{\gamma_e/(\gamma_e-1)} \tag{43}$$

Thus, setting $\dot{m}_e = \dot{m}_p + \dot{m}_s$, expanding the mass flow rate terms by Eq. (36), and solving for p_{te}/p_o

$$\frac{p_{te}}{p_o} = \frac{\left(\frac{\gamma_e+1}{2}\right)^{(\gamma_e+1)/[2(\gamma_e-1)]}}{\sqrt{\gamma_e/R_e}} \left[\frac{p_{tp}/p_o}{\sqrt{T_{tp}/T_{te}}} \frac{A_{pi}}{A} \sqrt{\frac{\gamma_p}{R_p}} \left(1+\frac{\gamma_p-1}{2}M_{pi}^2\right)^{-(\gamma_p+1)/[2(\gamma_p-1)]} + \right.$$
$$\left. \frac{p_{ts}/p_o}{\sqrt{T_{ts}/T_{te}}} \frac{A_{si}}{A} \sqrt{\frac{\gamma_s}{R_s}} \left(1+\frac{\gamma_s-1}{2}M_{si}^2\right)^{-(\gamma_s+1)/[2(\gamma_s-1)]} \right] \tag{44}$$

and

$$\frac{p_e}{p_o} = \frac{p_e}{p_{te}} \frac{p_{te}}{p_o} \tag{45}$$

Closure of the iteration process is then obtained by iterating the value of p_i/p_0 until the following relation from the conservation of momentum equation is satisfied

$$\frac{p_e}{p_o}(1+\gamma_e) \Bigg/ \left\{ \frac{p_i}{p_o} \left[\frac{A_{pi}}{A}\left(1+\gamma_p M_{pi}^2\right) + \frac{A_{si}}{A}\left(1+\gamma_s M_{si}^2\right) \right] \right\} = 1.0 \tag{46}$$

Finally, the ejector performance is obtained from

$$\phi_p = \frac{\dot{m}_e u_{10} - \dot{m}_s u_o}{\dot{m}_p u_{po}} = (1+\alpha)\frac{u_{10}}{u_{po}} - \alpha\frac{u_o}{u_{po}} \tag{47}$$

$$\frac{F}{\dot{m}_p} = \phi_p u_{po} \tag{48}$$

$$I_{sp} = \frac{\phi_p u_{po}}{g_o} \tag{49}$$

where

$$\frac{u_o}{u_{po}} = \frac{M_o}{M_{po}} \sqrt{\frac{\gamma_s R_s}{\gamma_p R_p}} \sqrt{\frac{T_{ts}/T_o}{T_{tp}/T_o}} \left[\frac{1+\frac{\gamma_p-1}{2}M_{po}^2}{1+\frac{\gamma_s-1}{2}M_o^2} \right]^{1/2} \tag{50}$$

$$\frac{u_{10}}{u_{po}} = \frac{M_{10}}{M_{po}} \sqrt{\frac{\gamma_e R_e}{\gamma_p R_p}} \sqrt{\frac{T_{te}/T_o}{T_{tp}/T_o}} \left[\frac{1+\frac{\gamma_p-1}{2}M_{po}^2}{1+\frac{\gamma_s-1}{2}M_{10}^2} \right]^{1/2} \tag{51}$$

IV. Validation

The predicted cycle time for the PDR agrees with observed cycle times for a 1 m long detonation engine that is currently being tested. Furthermore, the predicted end-wall pressures agree very well with measured end-wall pressures for an earlier PDR.[9] Comparisons of pressure and temperature distributions within the PDR also agree well with CFD simulations.[10] Furthermore, the performance trends predicted from the current model agree with trends predicted by the CFD simulations in Ref. 1.

V. Quasi-Steady Ejector Model vs. Cycle-Averaged Performance Model

Two models are employed for incorporating the unsteady primary flow from the PDR into the steady-flow ejector model. In the first model (Cycle Average Model), the cycle average pressure and temperature values given by Eqs. (52) and (53) for the PDR are used directly in the Heiser and Pratt steady-flow ejector analysis.

$$\bar{p}_{tp} = \frac{1}{t_3}\int_0^{t_3} p_{tp}\,dt \tag{52}$$

$$\bar{T}_{tp} = \frac{1}{t_3}\int_0^{t_3} T_{tp}\,dt \tag{53}$$

$$\bar{\pi}_{ejector} = \frac{1}{t_3}\int_0^{t_3} \pi_{ejector}\,dt \tag{54}$$

$$\bar{\phi}_p = \frac{1}{t_3}\int_0^{t_3} \phi_p\,dt \tag{55}$$

$$\overline{\left(\frac{F}{\dot{m}}\right)} = \frac{1}{t_3}\int_0^{t_3} \left(\frac{F}{\dot{m}}\right)dt \tag{56}$$

$$\bar{I}_{sp} = \frac{1}{t_3}\int_0^{t_3} I_{sp}\,dt \tag{57}$$

In the second model (Quasi-Steady Flow Model), the steady flow ejector calculations employ instantaneous values of pressure and temperature at specific times during the PDR cycle. Thus ejector performance is presented as a function of time and cycle average values are then obtained by integrating the instantaneous distributions over the entire cycle, Eqs. (54) – (57).

The time-averaged results from the quasi-steady flow model are quite close to the results of the cycle-averaged model, as shown in Fig. 7. These curves also show the cycle-averaged results from optimization studies of the ejector-augmented PDR that are discussed in more detail in the following section.

VI. PDR Optimization

The current analytical method is ideally suited for rapid, preliminary optimization of the performance of the ejector-augmented PDR. Two specific illustrative examples are shown in Figs. 8 and 9. Fig. 8 shows the effect of area ratio on ejector performance for a flight Mach number of 2. The area ratio is seen to have a significant effect on performance. An increase in area ratio causes a slight increase in ejector pressure ratio during the detonation part of the cycle; however, the pressure ratio falls more rapidly during the blow down part of the cycle at higher area ratios. Higher area ratios uniformly increase the instantaneous values of thrust augmentation ratio, specific thrust and specific impulse, leading to higher cycle-averaged values for each of these parameters, as shown in Fig. 7. For example, when the area ratio is increased from three to nine, the thrust augmentation ratio, the specific thrust and the specific impulse all increase by a factor of about two.

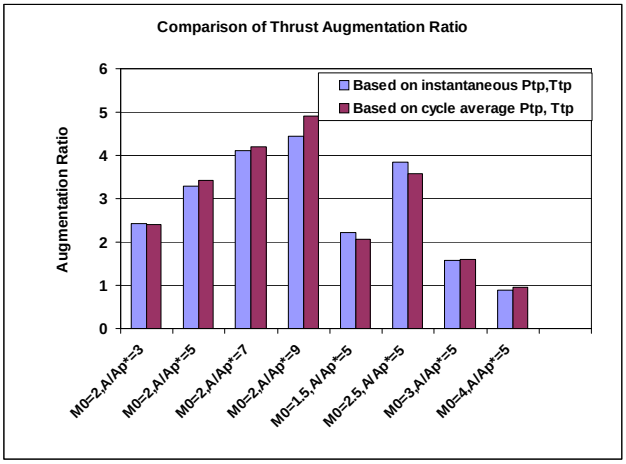

a. Augmentation ratio.

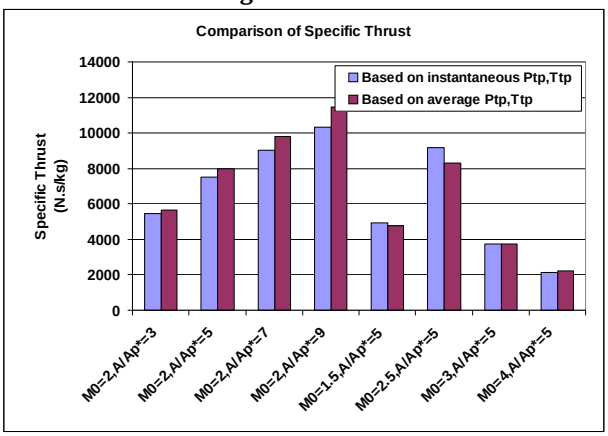

b. Specific thrust.

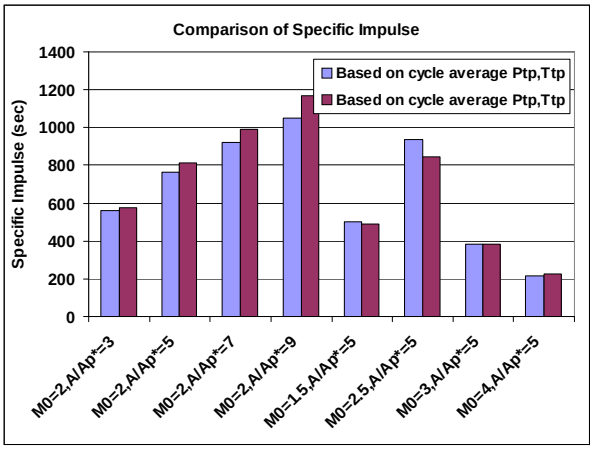

c. Specific impulse.

Figure 7. Comparison of ejector prediction methods.

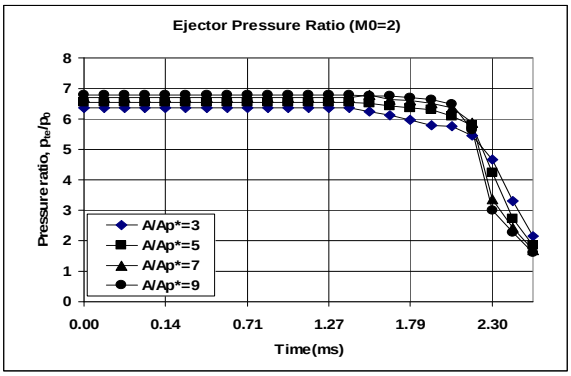

a. Ejector pressure ratio.

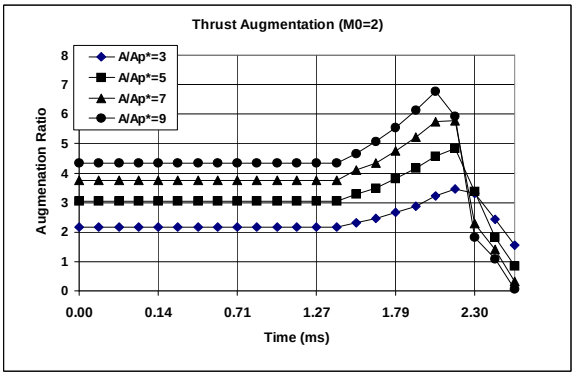

b. Augmentation ratio.

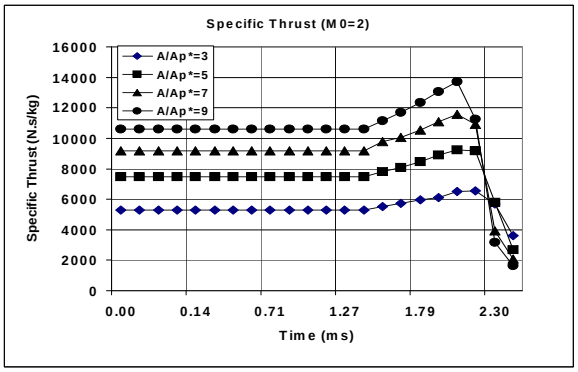

c. Specific thrust.

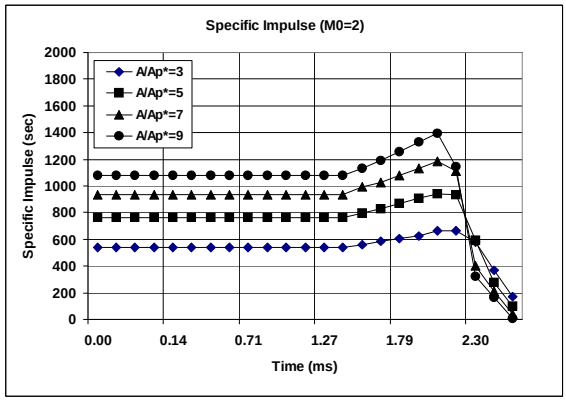

d. Specific impulse.

Figure 8. Effect of Area Ratio on Ejector Performance, $M_o = 2$.

Figure 9 shows the effect of flight Mach number on ejector performance for a fixed area ratio of five. The ejector pressure ratio initially increases with increased Mach number to a peak value at Mach 2.5 and then decreases as the Mach number continues to increase. Similar trends are observed in the augmentation ratio, specific thrust, and specific impulse.

VII. Performance Estimate for a Typical Constant q_o Trajectory

Figure 10 shows estimated performance for a typical constant dynamic pressure trajectory (q_o = 1000 lbf/ft^2 for an area ratio $A_p / A^* = 7$). The thrust augmentation ratio, specific thrust and specific impulse all increase with Mach number from takeoff up to Mach 2, and then decrease as the Mach number increases beyond 2.

VIII. Summary and Conclusions

An analytical model for predicting performance of an ejector-augmented pulse detonation rocket has been developed. The PDR performance is calculated using the Endo and Fujiwara model.[6] PDR performance is calculated at specific times during the PDR cycle, and the resulting end-wall pressure and temperature values are employed as the representative stagnation point values for the primary flow in the Heiser and Pratt steady flow ejector model.[7] The model is implemented via a spreadsheet, which allows for rapid performance estimates to be made for design optimization. Also, rapid performance estimates for representative trajectories are possible with this analytic tool. Performance parameters, such as the cycle time, end-wall pressures, and internal pressure and temperature distributions for the PDR agree well with our experimental data.

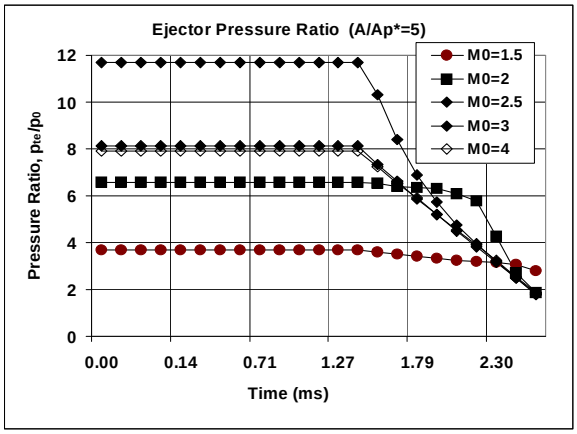

a. Ejector pressure ratio.

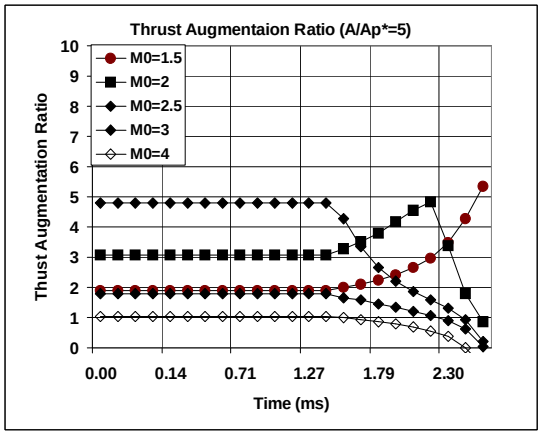

b. Augmentation ratio.

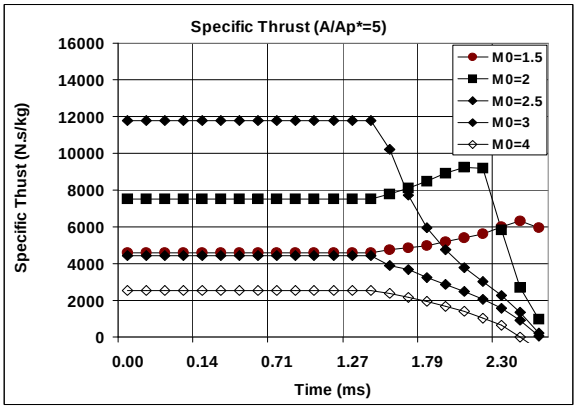

c. Specific thrust.

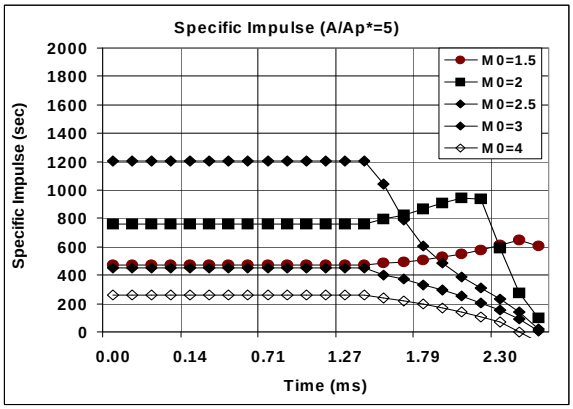

d. Specific impulse.

Figure 9. Effect of Mach number on ejector performance, $A/A_p^* = 5$.

Future improvements to the code will include replacing the assumed linear pressure decay during the blow down part of the cycle with a model that employs numerical integration of non-linear ordinary differential equations for dp_{tp}/dx and dT_{tp}/dx. These equations are derived from the integral form of the mass and energy conservation equations employing a classical uniform flow-uniform state model that has been used with great success to predict the blow down characteristics of supersonic wind tunnels. Furthermore, the model will be extended to include the purge and re-fill parts of the cycle.

References

[1]Munipalli, R., Shankar, V., Wilson, D.R., Kim, H., Lu, F.K. and Liston, G., "Performance Assessment of Ejector-Augmented Pulsed Detonation Rockets," AIAA Paper 2001–0830, 2001.

[2]Munipalli, R., Shankar, V., Wilson, D.R., Kim, H., Lu, F.K. and Hagseth, P.E., "A Pulsed Detonation Based Multimode Engine Concept," AIAA Paper 2001–1786, 2001.

[3]Munipalli, R., Shankar, V., Wilson, D.R., and Lu, F.K., "Preliminary Design of a Pulse Detonation Based Combined Cycle Engine," ISABE Paper 2001-1213, 15th International Symposium on Airbreathing Engines," Bangalore, India, September 2-7, 2001.

[4]Bussing, T. and Pappas, G., "An Introduction to Pulse Detonation Engines," AIAA Paper 94–0263, 1994.

[5]Gordon, S. and McBride, B.J., "Computer Program for Calculation of Complex Chemical Equilibrium Compositions, Rocket Performance, Incident and Reflected Shocks, and Chapman-Jouguet Detonations," NASA SP 273, 1971.

[6]Endo, T and Fujiwara, T., "Analytical Estimation of Performance Parameters of an Ideal Pulse Detonation Engine," *Transactions of the Japan Society for Aeronautical and Space Sciences*, Vol. 45, No. 150, 2003, pp. 249–254.

[7]Heiser, W. and Pratt, D., *Hypersonic Air Breathing Propulsion*, AIAA, 1994.

[8]*Model Specification for Engines, Aircraft, Turbojet*, Military Specification MIL-E-5006B, Department of Defense, January 1959.

9Stuessy, W.S. and Wilson, D.R., "Influence of Nozzle Geometry on the Performance of a Pulse Detonation Wave Engine," AIAA Paper 97–2745, 1997.

[10]Yi, T.H., Wilson, D.R. and Lu, F.K., "Detonation Wave Propagation in a Tube Embedded in a Combustion Chamber," AIAA Paper 2006–0953, 2006.

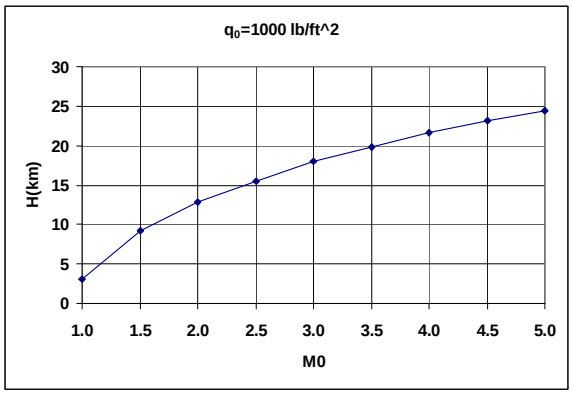

a. Constant dynamic pressure trajectory.

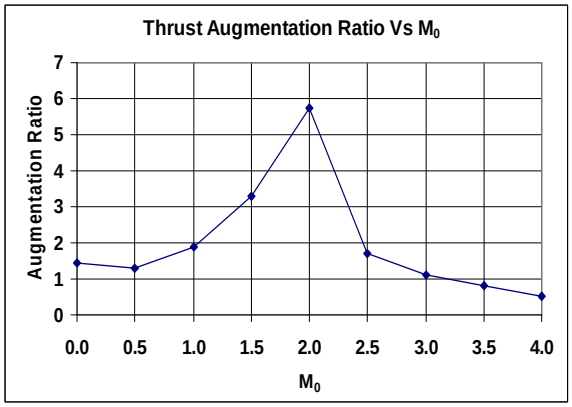

b. Augmentation ratio.

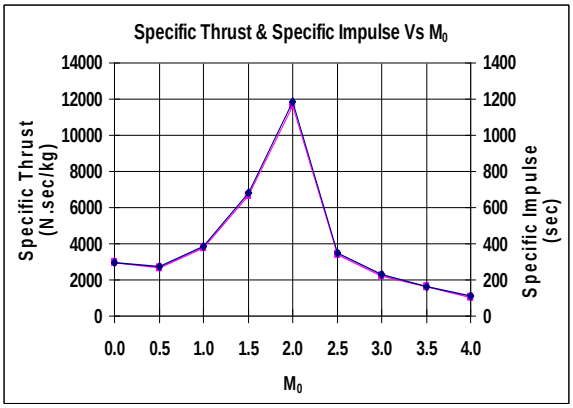

c. Specific thrust and impulse.

Figure 10. Ejector-augmented PDR performance for constant q_o trajectory, $A_p / A^* = 7$.